



High-pressure viscosity of liquid Fe and FeS revisited by falling sphere viscometry using ultrafast X-ray imaging



Yoshio Kono^{a,*}, Curtis Kenney-Benson^a, Yuki Shibazaki^b, Changyong Park^a, Guoyin Shen^a, Yanbin Wang^c

^aHPCAT, Geophysical Laboratory, Carnegie Institution of Washington, 9700 S. Cass Ave., Argonne, IL 60439, USA

^bFrontier Research Institute for Interdisciplinary Sciences, Tohoku University, Aramaki aza Aoba 6-3, Aoba-ku, Sendai 980-8578, Japan

^cGeoSoilEnviroCARS, Center for Advanced Radiation Sources, The University of Chicago, 5640 S. Ellis Avenue, Chicago, IL 60637, USA

ARTICLE INFO

Article history:

Received 18 August 2014

Received in revised form 25 November 2014

Accepted 16 February 2015

Available online 21 February 2015

Keywords:

Viscosity
Liquid iron
Liquid iron sulfide
High pressure
Liquid structure

ABSTRACT

The viscosity of liquid Fe and FeS has been extensively studied, yielding results differing by almost a factor of ten (2.4–23.7 mPa s for liquid Fe, 3.6–17.9 mPa s for liquid FeS, and 7.4–35.6 mPa s for the Fe–S eutectic composition), possibly due to the low resolution of slow cameras previously employed (typically 30–60 frames/s) in falling sphere measurements using X-ray radiography. Here we revisit the viscosity of liquid Fe and FeS up to 6.4 GPa using recently developed ultrafast X-ray imaging. In this study, we imaged the falling spheres at a rate of 500 frames/s, which is around 10 times faster than previous viscosity measurements. Our measurements showed that terminal velocity is achieved only in a limited region of falling distance, and that substantial oversampling, using sufficiently high-speed X-ray imaging, is essential to accurately determine the terminal velocity and the resulting viscosity. We obtained a viscosity of 6.1–7.4 mPa s for liquid Fe and 4.7–5.7 mPa s for liquid FeS at pressures to 6.4 GPa along their respective melting curves. The viscosity of liquid FeS is about 25–35% lower than that of liquid Fe between around 2 and 6.4 GPa along their respective melting curves. After correction for the effect of different melting temperatures between Fe and FeS on viscosity, we found that viscosity of liquid FeS is 31–42% lower than that of liquid Fe at 1800 °C and 1–6 GPa, suggesting that sulfur markedly decreases viscosity in liquid Fe.

© 2015 Elsevier B.V. All rights reserved.

1. Introduction

Viscosities of molten iron alloys are among the most fundamental properties required to understand the formation and dynamics of liquid outer cores in the Earth and other planets. It is thought that some planetary cores, including the Earth's, are mainly composed of liquid iron with certain light elements (e.g., Birch, 1964; Poirier, 1994; Stevenson, 2001; Weber et al., 2011). Efforts have been made to determine the viscosity of liquid iron-light element alloys at high pressures and high temperatures, particularly for liquid iron-sulfur alloys (LeBlanc and Secco, 1996; Dobson et al., 2000; Terasaki et al., 2001, 2002, 2006; Urakawa et al., 2001; Rutter et al., 2002; Perrillat et al., 2010). The pioneering study of LeBlanc and Secco (1996) reported a high viscosity of $1.6\text{--}43.6 \times 10^3$ mPa s for Fe-27 wt.% S liquid at 2–5 GPa and 1100–1300 °C using the falling sphere technique by analyzing probing sphere positions in samples quenched from high-pressure and high-temperature conditions. In contrast, later studies used an

in situ X-ray radiography technique to monitor the fall of the probing spheres and reported that liquid Fe–S alloys have very low viscosities around 10 mPa s, about 3 orders of magnitude lower than those reported by LeBlanc and Secco (1996). However, the reported results from these previous in-situ studies are also scattered, covering a range of almost one order of magnitude: 2.4–23.7 mPa s for liquid Fe (Terasaki et al., 2002; Rutter et al., 2002), 3.6–17.9 mPa s for liquid FeS (Dobson et al., 2000; Perrillat et al., 2010), and 7.4–35.6 mPa s for the eutectic Fe–S liquid (Dobson et al., 2000; Terasaki et al., 2001; Urakawa et al., 2001). For example for liquid Fe, Terasaki et al. (2002) reported an increase of viscosity with increasing pressure from 17.4 mPa s at 2.8 GPa and 1692 °C to 23.7 mPa s at 5.4 GPa and 1820 °C, and then a rapid decrease to about 6–9 mPa s at 6–7 GPa around 1900 °C, respectively. In contrast, Rutter et al. (2002) reported nearly constant low viscosity values of 2.36–4.80 mPa s at pressures between 1.6 and 5.5 GPa at a temperature close to 1777 °C. Precise viscosity measurements are required to understand the viscosity of liquid Fe–S alloys.

Falling sphere viscosity measurements are based on the Stokes' equation. The viscosity (η) can be calculated via the Stokes' equation with correction factors for the effect of both the wall (F)

* Corresponding author.

(Faxén, 1925) and the end (E) (Maude, 1961) of a cylindrical sample container:

$$\eta = \frac{g d_s^2 (\rho_s - \rho_l) F}{18 \nu \bar{E}} \quad (1)$$

$$F = 1 - 2.104 \left(\frac{d_s}{d_l}\right) + 2.09 \left(\frac{d_s}{d_l}\right)^3 - 0.95 \left(\frac{d_s}{d_l}\right)^5 \quad (2)$$

$$E = 1 + \frac{9}{8} \frac{d_s}{2Z} + \left(\frac{9}{8} \frac{d_s}{2Z}\right)^2 \quad (3)$$

where ρ and d are density and diameter, with subscripts s and l denoting properties of the probing sphere and liquid sample, respectively. Z is the sample height; ν is terminal velocity of the falling sphere. It has been pointed out that uncertainties in terminal velocity play a dominant role in the precision of the viscosity determination (Brizard et al., 2005). For liquid samples with identical sphere and container geometries, the precision of the terminal velocity measurement depends primarily on the camera frame rate. Previous high-pressure viscosity measurements were conducted using limited imaging rates (~ 30 – 60 frames/s (fps), except for 1 data point for liquid $\text{Fe}_{78}\text{S}_{22}$ in Terasaki et al. (2006), which had an imaging rate of 125 fps). Such low-speed imaging may be sufficient for studying viscous melts such as silicates or oxides, but it is insufficient to study less viscous liquids such as liquid Fe alloys. For example, some viscosity results were based on only 2–4 images of the falling balls (Dobson et al., 2000; Terasaki et al., 2001; Urakawa et al., 2001; Perrillat et al., 2010). Such limited imaging rates make it difficult to ensure that the falling sphere has reached terminal velocity and therefore result in large uncertainties in the calculated viscosity. On the other hand, Rutter et al. (2002) determined low viscosities by adopting a composite sphere having a similar density to that of the liquid sample in order to reduce terminal velocity. As a result, they were able to monitor the position of the sphere with sufficient sampling rate to determine terminal velocity. The drawback of this approach is that it magnifies a different source of uncertainty, since small uncertainties in the liquid density lead to large relative changes in the density difference between the liquid and the probing sphere. Since Rutter et al. (2002) did not measure liquid density and viscosity simultaneously, uncertainties in liquid density may be a significant source of errors in their reported viscosity. To minimize errors due to uncertainty in the density of the sample, it is important to use probing spheres that have a large density contrast relative to the sample liquid, but this, in turn, will result in high terminal velocities. To overcome this problem and to precisely determine the viscosities of less viscous liquids at high pressures, we have implemented a high-speed camera that can collect images at a rate of more than 1000 fps (e.g., Kono et al., 2013, 2014a,b). Here we reexamine viscosities of Fe and FeS liquids up to 6.4 GPa by using the latest technique of viscosity measurement.

2. Experiments

Viscosity measurements were conducted in a Paris-Edinburgh (PE) cell at the 16-BM-B beamline of the High Pressure Collaborative Access Team (HPCAT) at the Advanced Photon Source. We used a standard PE cell assembly (cf. Kono et al., 2014a) with a cylindrical sample enclosed in a BN capsule. The diameter of the sample was 1.0 mm for Fe and 1.5 mm for FeS with a height of 2.0 mm for both samples. We used Fe (99.9% purity, Sigma–Aldrich) and FeS (99.9% purity, Sigma–Aldrich) powder as starting materials, which were compacted into cylinders with the stated dimensions and compressed in the PE cell prior to melting. Temperatures were estimated based on power–temperature curves that were

determined in a separate experiment using an identical cell configuration (Kono et al., 2014a). The estimated temperatures were consistent with the melting curve of Fe (Strong et al., 1973) with a standard deviation of 20 °C (Fig. 1), similar to those of previous study (Kono et al., 2013) confirmed by the melting curves of NaCl and KCl (standard deviation of 50 °C at pressures up to 7.3 GPa). Pressures were determined by the equation of state of MgO (Kono et al., 2010). Details of the Paris-Edinburgh cell high-pressure and high-temperature experiment are described in Kono et al. (2014a).

Falling-sphere viscosity measurements were carried out through X-ray radiography using a high-speed camera (Photron SA3). The pixel size of the high-speed camera ($5.46 \pm 0.01 \mu\text{m}/\text{pixel}$) was calibrated by using a 497 μm WC ball as a scale reference. In this study, we adopted a frame rate of 500 fps with 2 ms exposure time. Terminal velocities were determined with a standard deviation of 0.8–5.3%. Precise determination of the diameter of

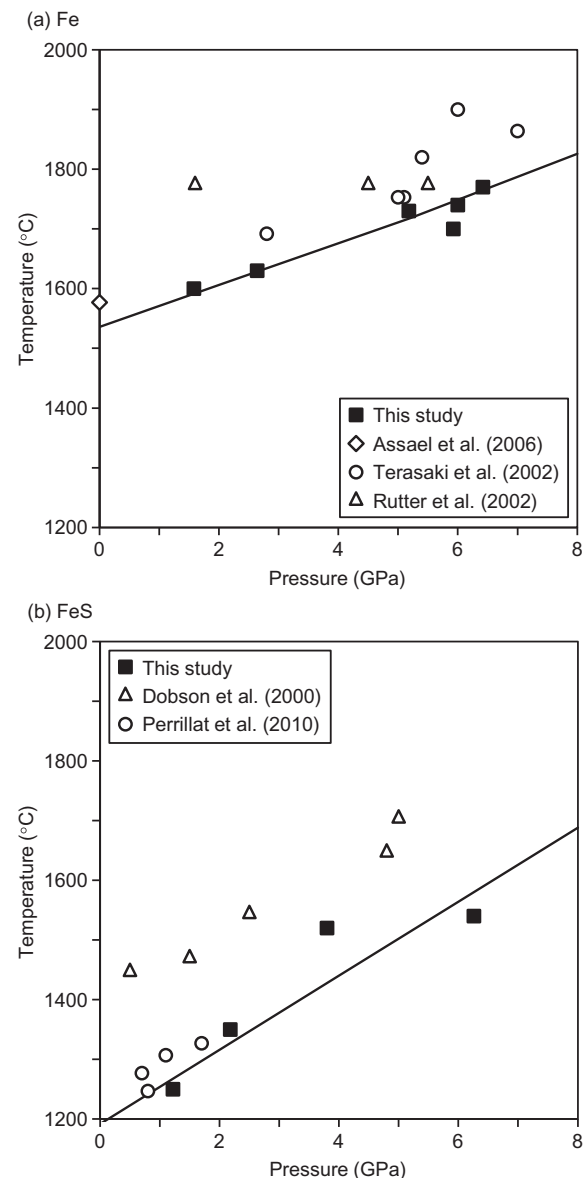


Fig. 1. Pressure and temperature conditions of viscosity measurements for liquid Fe (a) and FeS (b) in this study and previous studies shown with melting curves of Fe (Strong et al., 1973) and a natural pyrrhotite (38 wt.% sulfur) (Sharp, 1969), respectively.

the probing sphere is also important for accurately determining viscosity. Diameters of the probing spheres were determined by using high-resolution X-ray imaging with 2 μm resolution (cf. Kono et al., 2014a) for the liquid FeS experiment. In the liquid Fe experiment, we found that the sphere size decreased before the ball dropped, probably due to dissolution of the W95%Re5% sphere into the liquid Fe. Since the volume of the liquid sample (1 mm diameter and 2 mm height) is significantly larger than the size of the sphere (up to 0.131 mm in diameter), the dissolution of sphere material into the liquid Fe would cause negligible influence on the density of liquid Fe. On the other hand, determination of sphere diameter during falling is important to precisely determine viscosity. Fortunately, we confirmed that the sphere size did not change while it fell, probably because of the short time (up to ~ 200 ms) required for the drop. The diameter of the sphere was determined using the high-speed camera image during falling with 5.46 μm resolution. The low image resolution causes large uncertainty in the viscosity measurement for liquid Fe. Errors in the diameter of the spheres yield 2.2–3.2% uncertainty in the viscosity of liquid FeS and 6.4–11.8% uncertainty in that of liquid Fe. In order to calculate viscosity, we used the density of liquid FeS calculated from the equation of state by Nishida et al. (2011). The density of liquid Fe was calculated by using the thermal expansion coefficient at ambient pressure (Hixson et al., 1990) and the bulk modulus reported by Jing et al. (2014). For the density of the probing sphere, we calculated density of a W95%Re5% sphere by using the reference density of 19.4 g/cm^3 at ambient condition combined with the equation of state for tungsten (Dorogokupets and Oganov, 2007). The overall uncertainty in our viscosity determination is up to 4.7% for liquid FeS and up to 15.6% for liquid Fe.

3. Results and discussion

3.1. Importance of ultrafast imaging in determining viscosity accurately

Fig. 2 shows a series of images representing the path of a W95%Re5% sphere falling through liquid FeS at 2.2 GPa and 1350 $^{\circ}\text{C}$. We analyzed the position of the sphere in each frame by using the Tracker plugin in the imaging analysis software ImageJ. The motion of the falling sphere could be monitored with significant oversampling by using the high-speed camera. Although the distance-versus-time plot appears, to the eye, to have a large linear segment, a careful analysis of the time derivatives shows that terminal velocity has been achieved only within a limited region of the falling distance (~ 0.95 – 1.20 mm) (Fig. 2b). It is difficult to identify this terminal velocity using the slower frame rates employed in previous viscosity measurements. In order to appreciate the influence of the camera frame rate on the determination of terminal velocity, we simulated the previous falling velocity analyses with varying camera frame rates, by removing certain recorded images periodically (Fig. 3). At a frame rate of 200 fps, it is possible to identify 4 data points with about the same falling velocity (Fig. 3d). However, no constant velocity region can be identified below 100 fps (Fig. 3a–c). In order to determine the terminal velocity accurately, it is essential to use ultrafast imaging and to confirm the region where terminal velocity is achieved by using substantially oversampled data.

In a previous study, Urakawa et al. (2001) suggested that the time and distance required to reach terminal velocity were short (9 ms and 36 μm , respectively) and negligible in the viscosity measurement for liquid Fe–FeS from a calculation. They estimated time and distance required to reach terminal velocity using the following equations, which were derived from Stokes' equation:

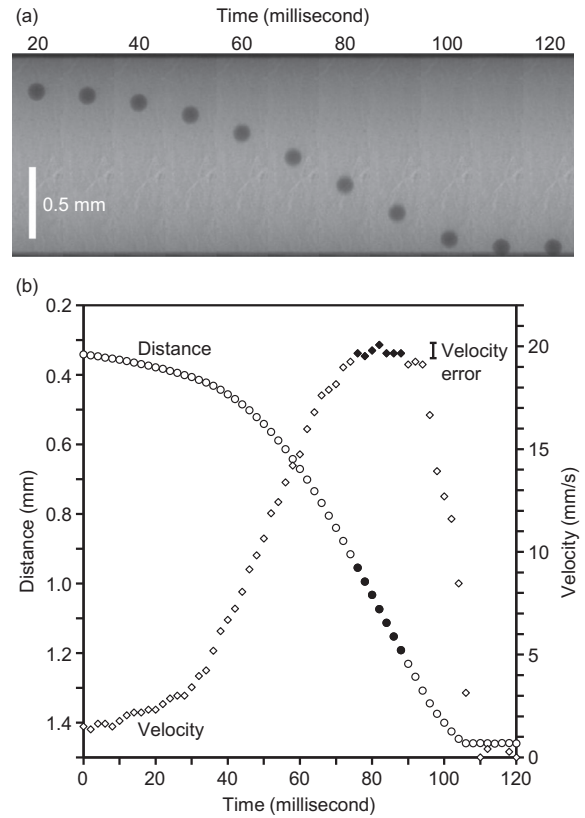


Fig. 2. X-ray radiography images of a falling W95%Re5% sphere (124 μm in diameter) in liquid FeS at 2.2 GPa and around 1350 $^{\circ}\text{C}$ (a) and the results of the falling distance analysis for each frame (2 ms interval). Terminal velocity was achieved only in a limited region of falling distance, indicated by solid symbols.

$$v(t) = (v_0 - v_T) \exp\left(-\frac{g(\rho_l - \rho_s)}{v_T \rho_s} t\right) + v_T \quad (4)$$

$$D(t) = -\frac{(v_0 - v_T)v_T \rho_s}{g(\rho_l - \rho_s)} \left(\exp\left(-\frac{g(\rho_l - \rho_s)}{v_T \rho_s} t\right) - 1\right) + v_T t \quad (5)$$

These equations represent the change of falling sphere velocity (v) with time (t) from the initial velocity ($v_0 = 0$) to the terminal velocity (v_T) and the resultant falling distance (D). Urakawa et al. (2001) calculated the time (9 ms) and distance (0.036 mm) required to reach terminal velocity by assuming $\rho_l = 6 \text{ g}/\text{cm}^3$, $\rho_s = 20 \text{ g}/\text{cm}^3$, and $v_T = -3.81 \text{ mm}/\text{s}$ in simulating the falling of a 50 μm diameter sphere in a liquid Fe–FeS having viscosity of 20 mPa s. We also calculated the time and distance required to reach terminal velocity for the experiment shown in Fig. 2 using the parameters $\rho_l = 4.6 \text{ g}/\text{cm}^3$, $\rho_s = 19.2 \text{ g}/\text{cm}^3$, $v_T = -19.7 \text{ mm}/\text{s}$, and obtained the time and distance to reach terminal velocity to be around 20 ms and 0.342 mm, respectively (Fig. 4). Although the simulation result is somewhat different from the experimental observation (the time and distance to reach terminal velocity was around 30 ms and around 0.5 mm in the experiment), the result clearly shows that the time and distance to reach terminal velocity are not negligibly short.

A factor that causes longer time and distance to reach terminal velocity in actual experiment may be incomplete melting, possibly due to heat transfer speed or minor temperature gradient in sample during the fall. In a falling sphere viscosity measurement for liquid NaCl, with a faster falling velocity of 53 mm/s (Kono et al., 2014a), the sphere fell immediately after melting, following a curved trajectory with non-uniform velocity profile; the sphere did not reach the terminal velocity. We interpret this behavior

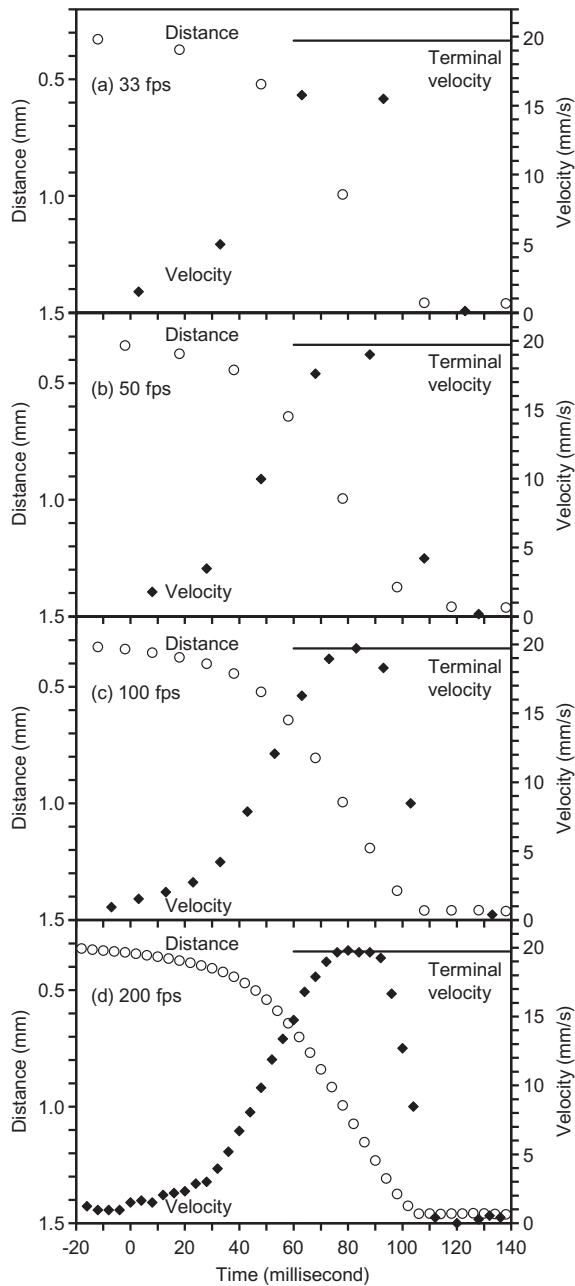


Fig. 3. A simulation of falling velocity analysis with varying camera frame rate. The terminal velocity obtained by 500 fps imaging (Fig. 2) is shown as a reference.

as due to the presence of (non-molten) NaCl crystals in the sample. In regions of a sample with incomplete melting, terminal velocity cannot be reached. Thus, it is important to monitor the motion of the sphere with high time resolution by using ultrafast imaging. Another way to avoid the influence of such incomplete melting is to release the probing sphere at sufficiently high temperature to ensure complete melting, by using a double-layer setup (e.g., Terasaki et al., 2001; Liebske et al., 2005). With this method, it is possible to avoid uncertainty of incomplete melting of sample. However, even when the sample is completely molten, it is still important to confirm terminal velocity. High-speed cameras provide the finer time resolution needed to accurately determine the terminal velocity.

The difference between Urakawa et al. (2001) and this study is mainly due to a difference in ball size (50 μm in the simulation of

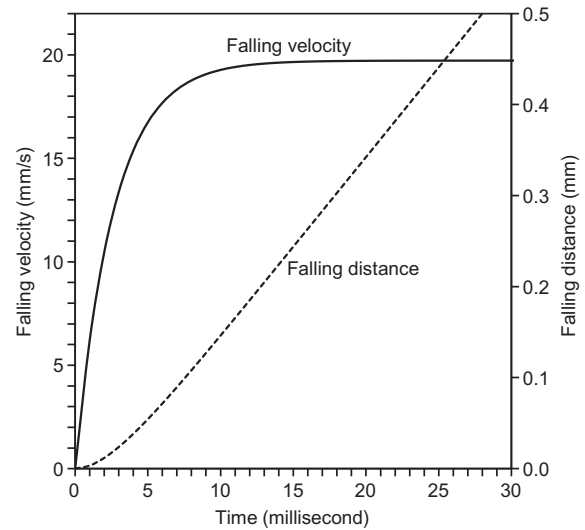


Fig. 4. Evolution of falling velocity with time and the resultant falling distance calculated by Eqs. (4) and (5), respectively.

Urakawa et al. (2001) and 124 μm in this study), which results in different terminal velocities. For the falling sphere measurement using a small ball size of 50 μm , the time and distance to reach terminal velocity may be negligible. However, a ball size of around 100–150 μm is common in previous falling sphere viscosity measurements (e.g., Urakawa et al., 2001; Terasaki et al., 2002, 2006). Actually, Urakawa et al. (2001) used a 100 μm ball in their falling sphere experiments, although they used 50 μm ball in the simulation. An examination of the impact of the different sphere sizes on terminal velocity, with other parameters in Eq. (1) held constant, shows that terminal velocity for a 100 μm sphere should be 4 times higher (15.24 mm/s) than the result in their simulation for a 50 μm sphere (3.81 mm/s). The high terminal velocity requires longer time (16 ms) and distance (0.21 mm) to be reached.

3.2. Viscosities of liquid Fe and FeS

Viscosity measurements are carried out up to 6.4 GPa at temperatures just above melting (Fig. 1), and the results are summarized in Table 1. Fig. 5 shows viscosities of liquid Fe (Fig. 5a) and liquid FeS (Fig. 5b) as a function of pressure along their respective melting temperatures. The viscosity for liquid Fe is found to be 6.1–7.4 mPa s, exhibiting a slight increase with increasing pressure

Table 1
Experimental conditions and the viscosity results.

Pressure (GPa)	Temperature ($^{\circ}\text{C}$)	Size of sphere (μm)	Terminal velocity (mm s^{-1})	Viscosity (mPa s)
<i>Fe</i>				
1.6	1600	82 \pm 2	5.7 \pm 0.2	6.1 \pm 1.0
2.6	1630	98 \pm 2	7.4 \pm 0.4	6.5 \pm 1.0
5.2	1730	131 \pm 2	10.5 \pm 0.5	7.1 \pm 0.8
5.9	1700	104 \pm 2	6.9 \pm 0.2	7.4 \pm 0.9
6.0	1740	87 \pm 2	6.1 \pm 0.2	6.4 \pm 1.0
6.4	1770	126 \pm 2	10.3 \pm 0.1	6.7 \pm 0.5
<i>FeS</i>				
1.2	1250	115 \pm 2	14.5 \pm 0.2	5.7 \pm 0.3
2.2	1350	124 \pm 2	19.7 \pm 0.2	4.8 \pm 0.2
3.8	1520	146 \pm 2	25.4 \pm 0.1	4.8 \pm 0.1
6.3	1540	106 \pm 2	14.7 \pm 0.2	4.7 \pm 0.2

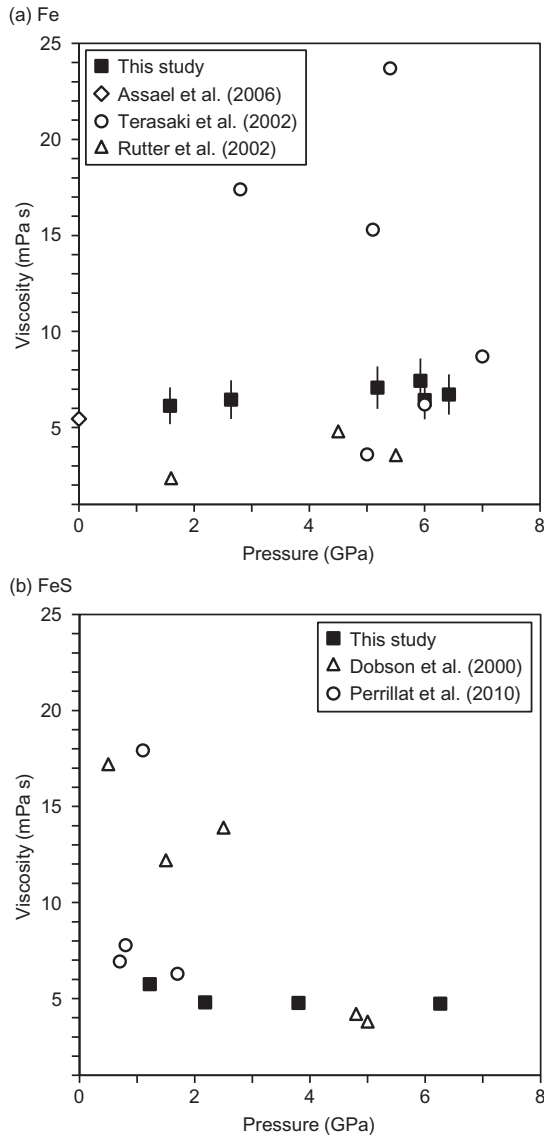


Fig. 5. Viscosity of liquid Fe (a) and FeS (b) as a function of pressure up to 6.4 GPa along their respective melting curves, compared with those reported by previous studies.

from 6.1 mPa s at 1.6 GPa to 7.4 mPa s at 5.9 GPa (Fig. 5a). The viscosity results of liquid Fe are fitted to the Arrhenius equation of pressure (P , in GPa) and temperature (T , in Kelvin):

$$\eta = \eta_0 \exp \left[\frac{Q + P \times \Delta V}{RT} \right] \quad (6)$$

where η_0 is viscosity at a reference condition; R is the gas constant; and activation energy Q and activation volume ΔV are fitting coefficients. Activation energy Q is fixed as 51.6 kJ/mol, which is derived by fitting the viscosity data at ambient pressure reported by Assael et al. (2006) in an equation:

$$\eta = \eta_0 \exp \left[\frac{Q}{RT} \right] \quad (7)$$

Fitting of the viscosity results of liquid Fe to the Eq. (6) with a fixed Q of 51.6 kJ/mol yields η_0 of 0.20 ± 0.01 mPa s and ΔV of $1.29 \pm 0.19 \times 10^{-6}$ m³/mol. The viscosity equation for liquid Fe yields 5.70 mPa s at ambient pressure and 1577 °C, which is in agreement with the reported value (5.443 mPa s at 1577 °C) (Assael et al., 2006). Our obtained viscosity results for liquid Fe

are slightly higher than those of Rutter et al. (2002), but much lower than those of Terasaki et al. (2002) at pressures lower than 5 GPa (Fig. 5a). Terasaki et al. (2002) suggested a strong decrease in the viscosity of liquid Fe from 23.7 mPa s to 3.6 mPa s at around 5 GPa. Although our data show a slight decrease in viscosity at around 6 GPa (Fig. 5a), the change is only ~ 1 mPa s and is within the size of errors.

The viscosity of liquid FeS is almost constant (4.7–4.8 mPa s) between 2.2 and 6.3 GPa, with a slightly higher value (5.7 mPa s) at 1.2 GPa. Our data are lower than those of previous studies (Dobson et al., 2000; Perrillat et al., 2010) up to ~ 3 GPa, with the temperature conditions of this study similar to those of Perrillat et al. (2010) and lower than those of Dobson et al. (2000). At higher pressures, our results are in consistent with those (3.8–4.2 mPa s at 4.8–5.0 GPa and 1650–1707 °C) reported in Dobson et al. (2000). Similarly to liquid Fe, viscosity data of liquid FeS are fitted to Eq. (6) with fixed Q of 29.8 kJ/mol, which is obtained by fitting an ambient pressure viscosity data reported by Barmin et al. (1970) in the Eq. (7). We obtain η_0 of 0.50 ± 0.05 mPa s and ΔV of $0.69 \pm 0.30 \times 10^{-6}$ m³/mol.

The effect of sulfur on the viscosity of liquid Fe–S alloys is controversial in previous studies. Dobson et al. (2000) studied viscosity of liquid FeS (36 wt.% S) and Fe–27 wt.% S, and suggested an increase in viscosity of liquid Fe–S alloy with increasing sulfur content. In contrast, Terasaki et al. (2001) proposed that sulfur decreases the viscosity of liquid Fe–S alloy from viscosity measurement for liquids Fe–12.6 wt.% S, Fe–19.8 wt.% S, and Fe–27.7 wt.% S. On the other hand, Perrillat et al. (2010) argued that the difference in viscosity between liquid Fe and FeS is insignificant. Our results clearly show that, while the viscosities of liquid Fe and FeS are similar at around 1.5 GPa (6.1 mPa s at 1.6 GPa for liquid Fe and 5.7 mPa s at 1.2 GPa for liquid FeS), viscosities of liquid FeS are lower by around 25–35% than those of liquid Fe at pressures between 2 and 6.4 GPa along their respective melting temperatures (Fig. 6). Since the temperature conditions of liquid FeS are lower than those of liquid Fe due to the lower melting temperature of FeS, the viscosity differences at comparable temperatures would be larger than those found in the experimental results. In order to understand the viscosity difference at the same temperature condition, we calculated the viscosity of liquid Fe and

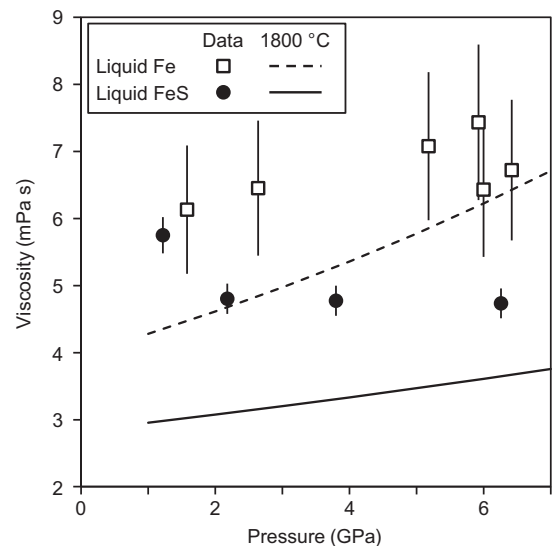


Fig. 6. Viscosities of liquid Fe and FeS obtained in this study. Lines represent viscosity of liquid Fe (broken line) and liquid FeS (solid line) at 1800 °C calculated by Eq. (6) using the obtained parameters.

FeS at 1800 °C using Eq. (6) and the obtained parameters. The data show that viscosity of liquid FeS is 31–42% lower than that of liquid Fe at 1800 °C and in a pressure range between 1 and 6 GPa (Fig. 6). This estimation depends on the activation energy. Our adopted activation energy value for liquid FeS (29.8 kJ/mol) is similar to those of Fe-27.7 wt.% S (30.0 kJ/mol) by Terasaki et al. (2001) and of FeS (35 kJ/mol) by Perrillat et al. (2010), while Dobson et al. (2000) reported a significantly higher value of 100 kJ/mol for Fe-27 wt.% S and 255 kJ/mol for FeS. Determinations of the activation energy and activation volume obtained by fitting viscosity data taken at high pressure and high temperature conditions are strongly interdependent. If a higher activation energy is used, the estimated activation volume will be different. In order to accurately determine activation energy and activation volume and to discuss the effect of sulfur content on viscosity precisely, it may be necessary to conduct systematic experiment at isothermal and isobaric conditions. Nevertheless, the fact that viscosities of liquid FeS obtained at lower temperatures (1350–1540 °C) is much lower than those of liquid Fe obtained at higher temperatures (1630–1770 °C) (Fig. 6) suggests that sulfur markedly decreases viscosity of liquid Fe.

3.3. Structural change in liquid Fe and liquid FeS at high pressures and its correlation with viscosity

A previous study of Sanloup et al. (2000) reported a structural change in liquid Fe in the vicinity of the δ - γ -liquid triple point (around 5.2 GPa, 1718 °C; Strong et al., 1973). At similar pressure and temperature conditions, Terasaki et al. (2002) showed a strong change in viscosity. However, our result does not show clear evidence of a viscosity change around the δ - γ -liquid triple point. In order to investigate the possible existence of a structural change in liquid Fe and the correlation of such a transition with a viscosity change, we measured the structure of liquid Fe just after the viscosity measurement using a multi-angle energy dispersive X-ray diffraction measurement by collecting diffraction patterns at 2θ angles of 2.5°, 3°, 4°, 5°, 7°, 10°, 13°, 18°, and 23° (Kono et al., 2014a). Unfortunately, we failed to obtain structure data at 5.2 GPa because the liquid sample leaked during the long data collection.

Fig. 7a shows the pair distribution function $G(r)$ of liquid Fe. Sanloup et al. (2000) showed an appearance of two distinct peaks at the 2nd peak position at high pressures, and suggested a

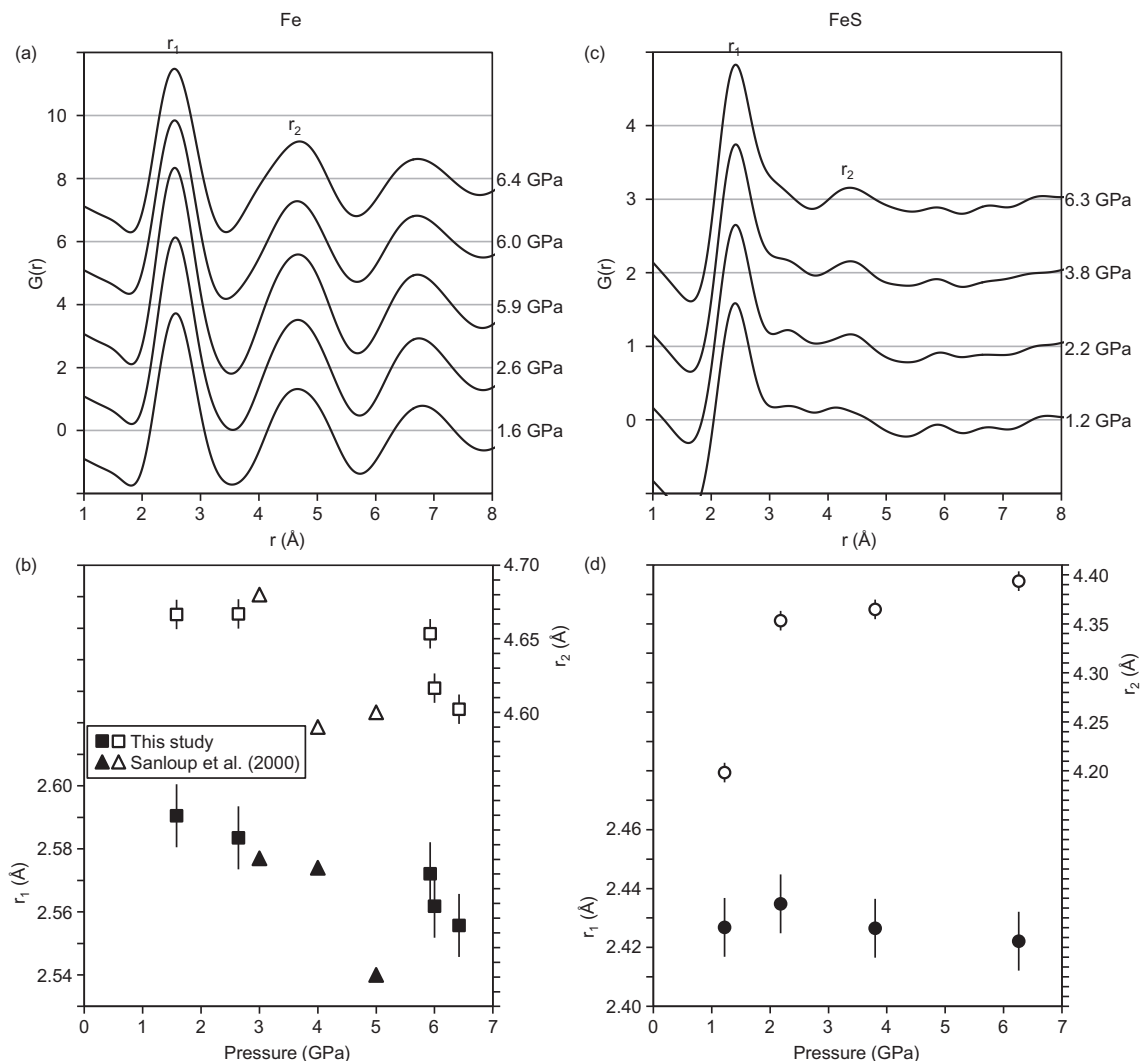


Fig. 7. The reduced pair distribution function $G(r)$ of liquid Fe (a) and FeS (c) at high pressures, and the first (r_1) and second (r_2) peak positions of liquid Fe (b) and FeS (d) as a function of pressure. The position of r_2 in liquid Fe was determined by the integrated mean in the same way as Sanloup et al. (2000).

structural change from bcc-like local order structure to a mixture of bcc- and fcc-like local order structure at high pressure and high temperature. However, our data showed no distinct peak splitting in the 2nd peaks even at the highest pressure condition. We observed slight broadening in the width of the 2nd peaks above 6 GPa. Fig. 7b shows positions of the 1st (r_1) and 2nd (r_2) peaks as a function of pressure. The r_2 distance showed marked decrease at 6 GPa in our data, and the r_1 distance also decreased slightly. The decrements of the r_1 and r_2 distances obtained in this study are similar to those of Sanloup et al. (2000) (Fig. 7b), although the pressure condition is different due to a different temperature condition. These data show that the structural change from the bcc-like structure to the bcc+fcc-like structure suggested by Sanloup et al. (2000) is not identified in our experiments, while there is change in the r_1 and r_2 distances at 6 GPa.

The structure of liquid FeS was also investigated just after the viscosity measurements (Fig. 7c and d). The r_1 distances showed no remarkable change up to 6.3 GPa, while the r_2 peak shows marked change with increasing pressure. Similar to previous studies for the structure of liquid Fe–S alloys (Urakawa et al., 1998; Sanloup et al., 2002; Morard et al., 2007), the r_2 peak is broad at low pressures, which implies that sulfur breaks intermediate range order in liquid Fe with moderate sulfur content at low pressures. The r_2 peak sharpens with increasing pressure probably due to better local ordering. This result is in agreement with Morard et al. (2007). In addition, the r_2 distance significantly increases at 1.2–2.2 GPa. Similarly, the viscosity of liquid FeS shows marked change between 1.2 GPa and higher pressures. It is difficult to discuss detailed effects of structure on viscosity, because the experiments were made along the melting curve. However, the correlation between structure and viscosity changes suggest that the shorter r_2 distance at 1.2 GPa may be the cause of the difference in the viscosity between 1.2 GPa and higher pressures. The possibility of a structural change in liquid FeS at low pressure was suggested by Nishida et al. (2011) as a cause of significant increase of density of liquid FeS between 0 and 0.5 GPa. Both our obtained viscosity change and the density change observed by Nishida et al. (2011) may be attributed to the change of r_2 distance.

4. Concluding remarks

We revisited the viscosity of liquid Fe and FeS by using an advanced technique of falling sphere viscosity measurement with ultrafast synchrotron X-ray imaging. Our data clearly show that monitoring the sphere motion with substantial oversampling is important to identify terminal velocity for the falling sphere and to accurately determine the resultant viscosity. Ultrafast imaging with sufficiently high camera frame rate is essential to investigate viscosity of low viscous liquids such as liquid Fe and Fe-light element alloys. Since viscosity measurements were conducted using frame rates of ~ 30 frames/s in early 2000's, these viscosity results, particularly for less viscous liquids, may contain large uncertainties due to the limited frame rate. Later, the viscosity measurements were carried out with improved frame rate of 60–125 frames/s in 2005–2006 (e.g., Liebske et al., 2005; Terasaki et al., 2006). In the present day, viscosity measurement with much higher frame rate of up to 2000 frames/s (this study; Kono et al., 2013, 2014b) enables us to precisely measure viscosity of less viscous liquids at high pressures.

Acknowledgements

We acknowledge two anonymous reviewers for valuable comments. The experiments were carried out at the Sector 16-BM-B,

HPCAT at the Advanced Photon Source. This research is supported by DOE-NNSA under Award Nos. DE-NA0001974 and DOE-BES under Award No. DE-FG02-99ER45775. The Advanced Photon Source is a U.S. Department of Energy (DOE) Office of Science User Facility operated for the DOE Office of Science by Argonne National Laboratory under Contract No. DE-AC02-06CH11357. YW acknowledges NSF Grant EAR-1214376.

References

- Assael, M.J., Kakosimos, K., Banish, R.M., Brillo, J., Egry, I., Brooks, R., Quedstedt, P.N., Mills, K.C., Nagashima, A., Sato, Y., 2006. Reference data for the density and viscosity of liquid aluminum and liquid iron. *J. Phys. Chem. Ref. Data* 35, 285–300.
- Barmin, L.N., Esin, O.A., Dobrovin, I.E., 1970. Application of theory of regular solutions to isotherms of viscosity and molar volume in binary sulphide melts. *Russ. J. Phys. Chem. USSR* 44, 1450–1453.
- Birch, F., 1964. Density and composition of mantle and core. *J. Geophys. Res.* 69, 4377–4388.
- Brizard, M., Megharfi, M., Verdier, C., 2005. Absolute falling-ball viscometer: evaluation of measurement uncertainty. *Metrologia* 42, 298–303.
- Dobson, D.P., Crichton, W.A., Vocadlo, L., Jones, A.P., Wang, Y., Uchida, T., Rivers, M., Sutton, S., Brodholt, J.P., 2000. In situ measurement of viscosity of liquids in the Fe–FeS system at high pressures and temperatures. *Am. Mineral.* 85, 1838–1842.
- Dorogokupets, P.I., Oganov, A.R., 2007. Ruby, metals, and MgO as alternative pressure scales: a semiempirical description of shock-wave, ultrasonic, X-ray, and thermochemical data at high temperatures and pressures. *Phys. Rev. B* 75, 024115.
- Faxén, H., 1925. Gegenseitige Einwirkung zweier Kugeln, die in einer zähen Flüssigkeit fallen. *Arkiv för Matematik, Astronomi och Fysik* 19, 1–8.
- Hixson, R.S., Winkler, M.A., Hodgdon, M.L., 1990. Sound speed and thermophysical properties of liquid iron and nickel. *Phys. Rev. B* 42, 6485.
- Jing, Z., Wang, Y., Kono, Y., Yu, T., Sakamaki, T., Park, C., Rivers, M.L., Sutton, S.R., Shen, G., 2014. Sound velocity of Fe–S liquids at high pressure: Implications for the Moon's molten outer core. *Earth Planet. Sci. Lett.* 396, 78–87.
- Kono, Y., Irfune, T., Higo, Y., Inoue, T., Barnhoorn, A., 2010. P–V–T relation of MgO derived by simultaneous elastic wave velocity and in situ X-ray measurements: A new pressure scale for the mantle transition region. *Phys. Earth Planet. Inter.* 183, 196–211.
- Kono, Y., Kenney-Benson, C., Park, C., Shen, G., Wang, Y., 2013. Anomaly in the viscosity of liquid KCl at high pressures. *Phys. Rev. B* 87, 024302.
- Kono, Y., Park, C., Kenney-Benson, C., Shen, G., Wang, Y., 2014a. Toward comprehensive studies of liquids at high pressures and high temperatures: combined structure, elastic wave velocity, and viscosity measurements in the Paris-Edinburgh cell. *Phys. Earth Planet. Inter.* 228, 269–280.
- Kono, Y., Kenney-Benson, C., Hummer, D., Ohfuji, H., Park, C., Shen, G., Wang, Y., Kavner, A., Manning, C.E., 2014b. Ultralow viscosity of carbonate melts at high pressures. *Nat. Commun.* 5, 5091. <http://dx.doi.org/10.1038/ncomms6091>.
- LeBlanc, G.E., Secco, R.A., 1996. Viscosity of an Fe–S liquid up to 1300° C and 5 GPa. *Geophys. Res. Lett.* 23, 213–216.
- Liebske, C., Schmickler, B., Terasaki, H., Poe, B.T., Suzuki, A., Funakoshi, K.-I., Ando, R., Rubie, D.C., 2005. Viscosity of peridotite liquid up to 13 GPa: implications for magma ocean viscosities. *Earth Planet. Sci. Lett.* 240, 589–604.
- Maude, A.D., 1961. End effects in a falling-sphere viscometer. *Br. J. Appl. Phys.* 12, 293–295.
- Morard, G., Sanloup, C., Fiquet, G., Mezouar, M., Rey, N., Poloni, R., Beck, P., 2007. Structure of eutectic Fe–FeS melts to pressures up to 17 GPa: implications for planetary cores. *Earth Planet. Sci. Lett.* 263, 128–139.
- Nishida, K., Ohtani, E., Urakawa, S., Suzuki, A., Sakamaki, T., Terasaki, H., Katayama, Y., 2011. Density measurement of liquid FeS at high pressures using synchrotron X-ray absorption. *Am. Mineral.* 96, 864–868.
- Perrillat, J.-P., Mezouar, M., Garbarino, G., Bauchau, S., 2010. In situ viscometry of high-pressure melts in the Paris-Edinburgh cell: application to liquid FeS. *High Pressure Res.* 30, 415–423.
- Poirier, J.-P., 1994. Light elements in the Earth's outer core: a critical review. *Phys. Earth Planet. Inter.* 85, 319–337.
- Rutter, M.D., Secco, R.A., Liu, H., Uchida, T., Rivers, M.L., Sutton, S.R., Wang, Y., 2002. Viscosity of liquid Fe at high pressure. *Phys. Rev. B* 66, 060102.
- Sanloup, C., Guyot, F., Gillet, P., Fiquet, G., Hemley, R.J., Mezouar, M., Martinez, I., 2000. Structural changes in liquid Fe at high pressures and high temperatures from synchrotron X-ray diffraction. *EPL (Eur. Lett.)* 52, 151–157.
- Sanloup, C., Guyot, F., Gillet, P., Fei, Y., 2002. Physical properties of liquid Fe alloys at high pressure and their bearings on the nature of metallic planetary cores. *J. Geophys. Res. Solid Earth* 107, 2272.
- Sharp, W.E., 1969. Melting curves of sphalerite, galena, and pyrrhotite and the decomposition curve of pyrite between 30 and 65 kilobars. *J. Geophys. Res.* 74, 1645–1652.
- Stevenson, D.J., 2001. Mars' core and magnetism. *Nature* 412, 214–219.
- Strong, H.M., Tuft, R.E., Hanneman, R.E., 1973. The iron fusion curve and γ - δ -I triple point. *Metall. Trans.* 4, 2657–2661.

- Terasaki, H., Kato, T., Urakawa, S., Funakoshi, K.-I., Suzuki, A., Okada, T., Maeda, M., Sato, J., Kubo, T., Kasai, S., 2001. The effect of temperature, pressure, and sulfur content on viscosity of the Fe–FeS melt. *Earth Planet. Sci. Lett.* 190, 93–101.
- Terasaki, H., Kato, T., Urakawa, S., Funakoshi, K., Sato, K., Suzuki, A., Okada, T., 2002. Viscosity change and structural transition of Molten Fe at 5 GPa. *Geophys. Res. Lett.* 29 (1227), 12. <http://dx.doi.org/10.1029/2001GL014321>.
- Terasaki, H., Suzuki, A., Ohtani, E., Nishida, K., Sakamaki, T., Funakoshi, K., 2006. Effect of pressure on the viscosity of Fe–S and Fe–C liquids up to 16 GPa. *Geophys. Res. Lett.* 33, L22307.
- Urakawa, S., Igawa, N., Kusaba, K., Ohno, H., Shimomura, O., 1998. Structure of molten iron sulfide under pressure. *Rev. High Pres. Sci. Tech.* 7, 286–288.
- Urakawa, S., Terasaki, H., Funakoshi, K., Kato, T., Suzuki, A., 2001. Radiographic study on the viscosity of the Fe–FeS melts at the pressure of 5 to 7 GPa. *Am. Mineral.* 86, 578–582.
- Weber, R.C., Lin, P.-Y., Garnero, E.J., Williams, Q., Lognonné, P., 2011. Seismic detection of the lunar core. *Science* 331, 309–312.